Journal of Materials Chemistry C

Accepted Manuscript

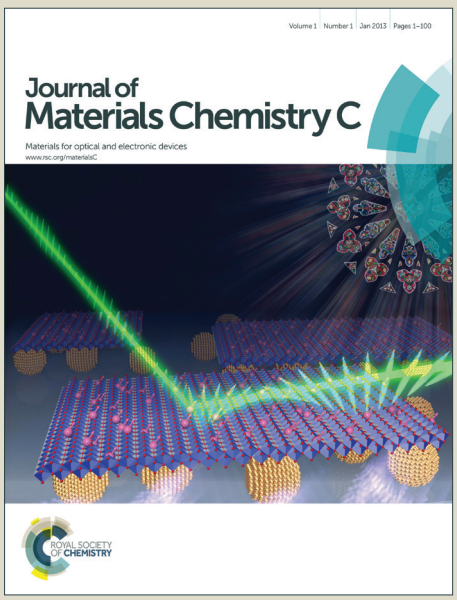

ROYAL SOCIETY OF CHEMISTRY

www.rsc.org/materialsC

Journal Name

RSCPublishing

ARTICLE

Facile synthesis of $Au_{23}(SC(CH_3)_3)_{16}$ clusters

Cite this: DOI: 10.1039/xoxxoooooox

Mahdi Hesari and Mark S. Workentin

Received ooth January 2012,
Accepted ooth January 2012

DOI: 10.1039/xoxxoooooox

www.rsc.org/

Mono-dispersed Au_{23} clusters protected by 16 tert-butyl thiols, a bulky-aliphatic ligand, have been synthesized using a one-pot protocol. The protocol yields two fractions in high yields. While both fractions are soluble in dichloromethane (and tetrahydrofuran, acetone, toluene), one can be isolated from the other by washing the solid mixture sample with acetonitrile. Electrospray ionization mass spectrometry showed accurate match between the experimental and simulated values, indicating $Au_{23}(SC_4H_9)_{16}$ for both fractions. MALDI MS experiments provide evidence that the core-shell structural formula consists of $Au(SR)_2$ and $Au_2(SR)_3$ units. The UV-Visible spectra of each fraction show a peak at 566 nm, with the HOMO-LUMO gaps of the acetonitrile and dichloromethane fractions being 1.88 and 1.94 eV, respectively. Both fractions show photoluminescence peak emission in the near-infrared region at 830 and 838 nm, for acetonitrile and dichloromethane fractions, respectively. The electrochemistry of the two fractions also revealed similar features, with irreversible peaks at 0.74 and -1.58 V *vs.* SCE resulting to an estimation of the HOMO-LUMO gap after charge correction of ca. 1.86 and 1.95 eV for acetonitrile and dichloromethane fractions, in close agreements with the optical values.

The noble metal nanostructures are important due to their utilization in catalysis,[1] photocatalysis,[2] and their optical,[3]magnetic,[4] and electrogenerated chemiluminescence properties.[5] Among different noble metal nanoclusters there is more focus on gold-based nanostructures due to their stability and proven applications in biological sensing,[6] supramolecular chemistry,[7] nanoelectrochemistry,[8] and therapeutic agents.[9] It has been shown that the gold nanoparticle/cluster size and properties can be altered by adjusting various parameters such as the ratio of metal to protecting ligand[10] and the synthetic conditions and solvent.[11] Importantly, the gold core properties can be tuned by the protecting ligands, mainly by altering the structure of the thiolate ligands.[12] The nature of the protecting ligand[13] induces various physicochemical properties in the small Au clusters, including the cluster core-sizes,[14] and the solubility,[15] electrochemical[16] and photochemical properties.[17] A key goal to the use of Au clusters is to be able to prepare them in good yield and as mono-dispersed products in a one-pot or other straightforward synthetic procedure. The Brust-Schiffrin method, the so-called two-phase method, is a well established protocol that utilizes a Au(I)-SR intermediate to make a wide range of gold nanoparticles. [18] In 2009 Jin and co-workers expanded the synthetic approach to an efficient one-pot synthesis procedure to make $Au_{25}(SR)_{18}$ clusters (SR= 2-phenylethanethiol, glutathione, 1-dodecanethiol) under kinetic controlled conditions.[19] Using either of these approaches and by controlling the formation of the Au(I)-SR intermediate and its subsequent reduction, there is opportunity to prepare different sized mono-dispersed gold clusters. For example, $Au_{20}(SC_2H_4Ph)_{16}$[20] and $Au_{24}(SC_2H_4Ph)_{20}$[21] have been prepared by simply adjusting the rate of addition of the reducing agent Using approaches like this, where either the Au:thiol ratio or the amount or the rate of addition of the reducing agent is altered a wide variety of Au clusters have been synthesized includingAu_{20},[14] Au_{25},[22] Au_{28},[23] Au_{36},[24] Au_{38}[25] and Au_{102},[26]

The nature of the protecting ligand(s) affect the surface properties and can dictate the type of nanostructure materials prepared.[27] For example, rare clusters such as Au_{44},[28] Au_{41},[29] Au_{36},[24, 30] Au_{30},[27, 31] Au_{39}, Au_{65}, and Au_{67}[31] are prepared using bulky protecting ligands. In addition to the protecting ligand structure (linear,[19] bulky,[32] aromatic[33] or aliphatic[34]) the ratio of gold to thiol plays a key role on the size and shape of the clusters.[10] The cluster structure and physical properties have also been studied theoretically but with simpler ligand such as sulfhydryl (-SH) or methyl thiol ($-SCH_3$) groups.[35-37] These simple ligands are extremely hard to handle experimentally, but 2-methyl-2-propanethiol, (tert-butyl thiol, $HSC(CH_3)_3$) is arguably one of the simplest bulky-aliphatic thiolate ligands and a cluster prepared from them would be useful models for some of these theoretical studies.[31] Lopez-Acevedo and Hakkinen predicted that smaller derivatives of $Au_{25}(SR)_{18}$ such as $Au_{19}(SR)_{12}^-$ could be experimentally prepared using bulky thiolate, such as tert-butyl thiol.[38] Recently, Dass and co-workers utilized $HSC(CH_3)_3$ in a two-step synthetic procedure using a 1:3 gold to thiol ratio and refluxing the intermediate cluster mixtures in the presence of excess of the neat thiol. They succeeded to separate a neutral $Au_{30}(SC(CH_3)_3)_{16}$ cluster that exhibited an unusual (compared to similar sized Au clusters) UV-Vis peak at 620 nm giving the cluster a green color. The purified $Au_{30}(SC(CH_3)_3)_{16}^0$ was separated using size-

exclusion chromatography (SEC) and was characterized by mass spectrometry techniques. More recently, Jin reported a $Au_{23}(SR)_{16}^-$ cluster decorated with cyclohexanethiol as the thiolate ligand derivatives.[39] The X-ray crystal structure clearly showed that the $Au_{23}(SR)_{16}^-$ cluster is composed of a Au_{15} kernel (cuboctahedron-based bipyramidal), protected by $2\times Au_3(SR)_4$, $2\times Au(SR)_2$ motifs, and 4×SR ligands.

In this report, we used $HSC(CH_3)_3$ as a stabilizing ligand and prepared novel Au_{23}^- clusters with a $Au_{23}(SC(CH_3)_3)_{16}$ structural formula. Our synthesis consists of one-phase/one-step procedure using $HSC(CH_3)_3$ as a bulky ligand and a higher gold to thiol ratio (1:6), at room temperature, which gave two negatively charged (Au_{23}^-) clusters in good yield. The final products were easily separated from the purified mixture through selective solvent extractions with acetonitrile and dichloromethane. The purified clusters were characterized by UV-Vis and NMR spectroscopy, Matrix-assisted laser desorption/ionization (MALDI) and electrospray ionization (ESI) mass spectrometry, electrochemistry and photoluminescence techniques.

Experimental

Chemicals. Gold (III) chloride trihydrate, 2-methyl-2-propanethiol, tetra-*n*-octylammonium bromide, tetrahydrofuran, sodium borohydride, and deuterated chloroform have been purchased from Aldrich. Reagent grade methanol was provided by BDH.

Characterization. UV-Vis spectra were recorded using a Cary 100 Bio instrument. The Gel Permeation Chromatography (GPC) instrument was equipped with a Viscotek GPC Max VE2001 solvent module. Samples were analyzed using the Viscotek VE3580 RI detector operating at 30°C. The separation technique employed two Agilent Polypore (300 7.5 mm) columns connected in series and to a Polypore guard column (50×7.5 mm). Samples were dissolved in THF (glass distilled grade) in approximately 5 mg/mL concentrations and filtered through 0.22 µm syringe filters. Samples were injected using a 100 µL loop. The THF eluent was filtered and eluted at 1mL/min for a total of 30 minutes. A calibration curve was obtained from polystyrene samples with molecular weight ranges of 1,540-1,126,000 g/mol ^{1}HNMR spectra were obtained on Inova 600 in $CDCl_3$. ESI mass spectra were measured using a Bruker miroTOF mass spectrometer. The sample was dissolved in dichloromethane and injected into the instrument capillary. MALDI-TOF spectra were collected on a BioAnalysis mass spectrometer, while laser intensity was kept at the lowest level, and the negative mode applied. The sample was dissolved in dichloromethane and mixed with *trans*-2-[3-(4-*tert*-Butylphenyl)-2-methyl-2-propenylidene] malononitrile (DCTB). Spotted samples air-dried prior to measurements. The sample to matrix ratio was adjusted at 1:1000. Powder X-ray diffraction of the $Au_{23}(SC_4H_9)_{16}^-$ cluster analyses was performed on a Rigaku rotating-anode X-Ray Diffractometer. The diffractometer employs Co (Kα) radiation, with monochromation achieved using a curved crystal, diffracted beam, graphite monochrometer. The instrument was operated at 45 kV and 160 mA, using the normal scan rate of 10° two-theta per minute (equivalent to 0.5° two-theta on conventional diffractometers). X-rays were collimated using 1° divergent and scatter slits, and a 0.15 mm receiving slit. Sample scans were completed from X to X° two-theta, at a rate of 10° /minute. Photoluminescence measurements were conducted in chloroform as solvent. The spectra were collected on an Andor 2300i spectrograph equipped with BB RD CCD camera. A green laser (532 nm) was used for the sample excitation. All the electrochemical experiments were conducted using a Autolab30 in dichloromethane as a solvent containing 0.1 M tetra-*n*-butylammonium hexafluorophosphate ($TBAPF_6$) as the supporting electrolyte. A home-made glassy carbon (GC) electrode served as working electrode (WE). The WE has been polished using 500, 1200, 2400 and 4000 grit paper. Fine polishing was performed using 1 and 0.5 micron diamond paste on a polishing cloth (Struers). A platinum counter electrode (CE) and a platinum wire quasi-reference electrode (RE) calibrated using ferrocene as an internal standard (0.342 V *vs.* SCE) were utilized.[40] Differential pulse voltammograms were obtained with peak amplitude of 50 mV, pulse width of 0.05 s, 2 mV increments per cycle, and a pulse period of 0.1 s.

RESULTS AND DISCUSSION

Synthesis, separation and UV-Vis of $Au_{23}(SC_4H_9)_{16}$.TOA clusters.

In a typical reaction 1.0 g (2.6 mmol) of gold (III) chloride trihydrate salt and 1.5 eq. tetra-*n*-octylammonium bromide co-dissolved in 100 mL tetrahydrofuran. The dark-orange mixture was cooled to 0°C (i) and then 6 eq. *tert*-butyl thiol was added to the mixture under slow stirring. Upon the thiol addition, and after 10 minutes the mixture color starts to change (ii), indicative of the expected -(-Au-SR-Au-)- polymer formation. After formation of a colorless solution within 50 minutes (iii), a fresh ice-cold sodium borohydride solution (10 eq.) was added with stirring. Upon addition of the reductant, the color of the solution turned to black (iv) an indication of nanocluster formation. The progress of the cluster formation was followed by optical absorption measurements, which show a peak formation at 566 nm as an indication of small cluster formation (Scheme 1). The solution was stirred until there was no change in the absorption at 566 nm roughly 18-26 hours. The reaction was then gravity filtered to remove unreacted Au(I)-SR intermediate and the solvent was removed by rotary evaporator. The excess of the thiol and sodium borohydride was removed through washing with a methanol: water mixture, leaving a dark-brown solid. The solid was transferred to a glass frit. It is worth noting that washing first with dichloromethane resulted in single fraction. However if first the solid was washed with acetonitrile a separate fraction with dark red color was isolated. The residual solid was then washed with dichloromethane, to extract a separate dichloromethane soluble (non acetonitrile soluble) fraction with a strong orange color. After removing the

solvent in dark red (~95 mg) and dark brown (~35 mg) solids formed on the wall of flasks for the acetonitrile and dichloromethane fraction, respectively. Both of the products are soluble in dichloromethane, chloroform, acetone, tetrahydrofuran, and toluene and the UV-Vis spectra show the same features in these solvents. The clusters also showed good solubility in non-polar solvents such as: hexane, heptane, and petroleum ether, likely the result of the presence of the short chain aliphatic ligand on the gold clusters surface.

The size and purity of both separated fractions was examined using SEC. Scheme 1 shows the SEC chromatograms of the acetonitrile fraction (A) and dichloromethane fraction (B) along with synthetic steps. The SEC experiment was performed using tetrahydrofuran as eluent; for details see experimental section.

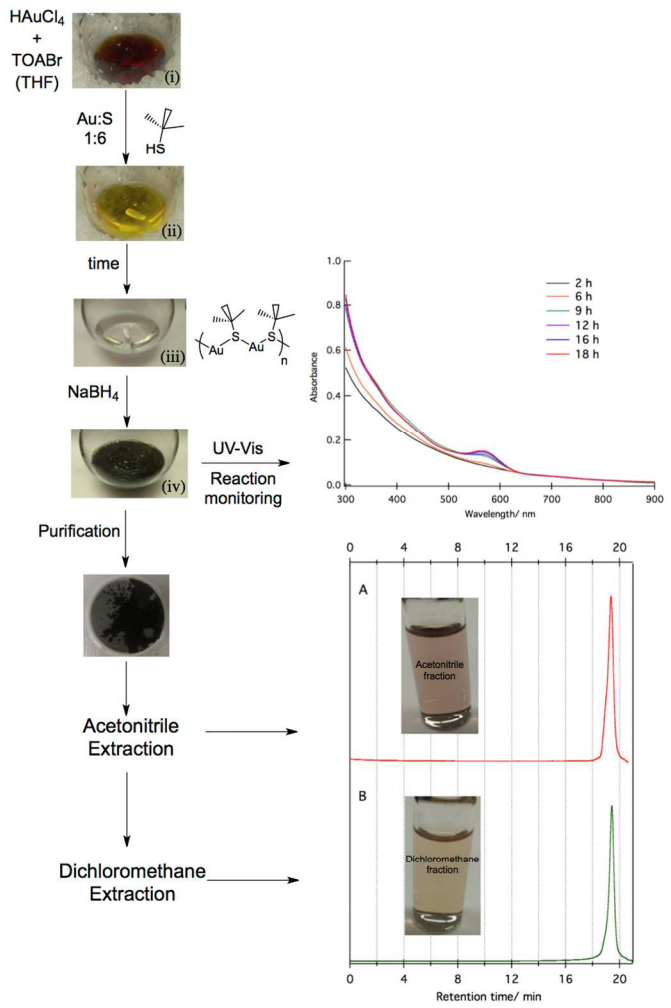

Scheme 1. Photographs of the synthetic steps are shown in the left panel. The tracked change in the UV-Vis spectra as a function of the reaction time is presented in the top right panel. SEC plots of the (A) acetonitrile and (B) dichloromethane fractions are shown in the bottom right panel (Insets show photographs of the resulting solutions).

The SEC spectra (A) and (B) each show a single peak at 19.39 and 19.43 min for acetonitrile and dichloromethane fractions, respectively, indicating the purity. The close retention times of fractions (A) and (B) represent the similarity of the size of both pure fractions.

Figure 1 shows the UV-Vis spectra of the acetonitrile (the black curve) and dichloromethane (the red curve) fractions measured in chloroform. Both fractions show very similar features with a peak at 566 nm and a valley at 490 nm (indicated with arrows in the panel a). It is worth nothing that there is a small difference in the peak intensity and depth of the valleys; the acetonitrile fraction revealed higher absorption at 566 nm and deeper valley at 490 nm.

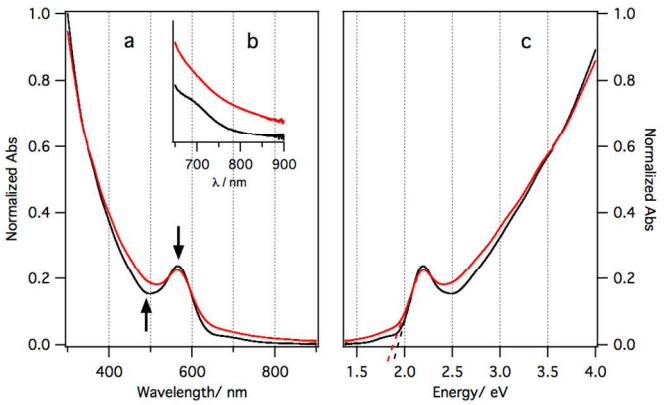

Figure 1. (a) UV-Vis spectra of the acetonitrile (the black curve), and dichloromethane (the red curve) fractions, (b) Expanded UV-Vis in the range of 650-900 nm, (c) Absorbance *vs.* energy (eV) of acetonitrile (the black curve), and dichloromethane (the red curve) fractions. All spectra were recorded in chloroform (C= 0.028 mM).

The UV-Vis peak's intercept gives an estimation of the optical HOMO-LUMO gap of *ca.* 1.88 and 1.94 eV for the acetonitrile and dichloromethane fractions, respectively. The peak at 566 nm is similar for both fractions, while they show very clear different intercepts indicative of slightly different HOMO-LUMO energy gaps. Furthermore, the acetonitrile fraction reveals a broad peak at 691 nm. The photographs of the samples are shown in Scheme 1. The optical HOMO-LUMO gap values agree with previously reported values for $Au_{20}(SC_2H_4Ph)_{16}$ (2.1 eV)[20] and $Au_{24}(SC_2H_4Ph)_{20}$ (1.5 eV).[21]

Mass spectrometry analysis.

Each of the acetonitrile and dichloromethane fractions cluster size and composition were evaluated using electrospray ionization (ESI) and Matrix assisted laser desorption/ionization (MALDI) mass spectrometry techniques. The ESI is a softer mass spectrometric technique relative to MALDI. Therefore, there is opportunity to observe the parent peak, while the combination of these two mass spectrometry techniques can be used to extract more structural details and evaluate different cluster compositions.[41-46] Representative ESI and MALDI-TOF mass experiments for both the acetonitrile and dichloromethane fractions are shown in Figure 2.

The fragile structure of tert-butyl thiolates on the surface of the clusters resulted in highly fragmented patterns in both the ESI and MALDI spectra. ESI spectra show a peak at 5954.9 Da corresponding to the intact mass value of $Au_{23}(SC(CH_3)_3)_{16}$.

The expansions of the parent peaks are shown as insets in panels (I) and (III) for acetonitrile and dichloromethane fractions. The high-resolution

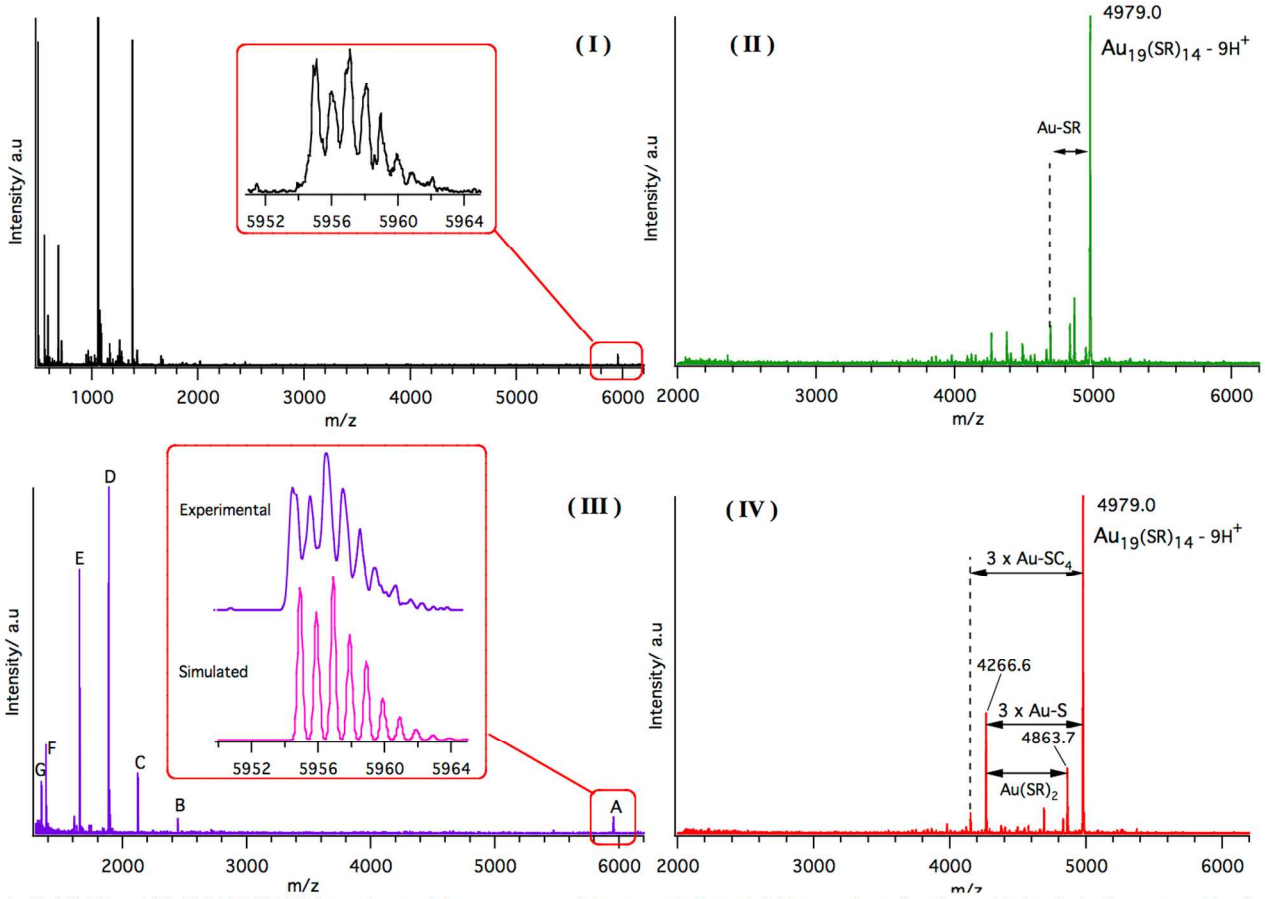

Figure 2. (I), (III) ESI and (II), (IV) MALDI-TOF (negative mode) mass spectra of the acetonitrile and dichloromethane fractions.with $Au_{23}S_{16}C_{64}H_{144}$ composition formula. A-G are peak assigned as fragments are expanded in the supporting information. The ESI insets show expanded parent experimental peaks for both fractions. The simulated isotopic patters for $Au_{23}(SC(CH_3)_3)_{16}$ is shown in panel (III) in comparison to the experimental pattern.

isotopic experimental and simulated patterns are shown in the inset of Figure 2, panel (III).

The experimental and simulated isotopic patterns for $Au_{23}(SC(CH_3)_3)_{16}$ are in an excellent agreement, providing confirmation of the proposed compositional structure. The ESI fragments of the dichloromethane fraction are also shown in Figure S1 A-G. There are multiple fragments, appearing at 5954, 2446, 2123, 1889, 1654, 1383.8 and 1346.0 Da. The MALDI spectra of both fractions are also shown in Figure 2 panel (II) and (IV). Each show a peak with 4979.0 Da, proposing $Au_{19}(SC_4H_9)_{14}$-$9H^+$. Further analysis of the ESI and MALDI spectra, given a mass difference value equal to 978 Da (*ca*. 980.256Da), accounts for 2 staple motifs with each containing –(SR-Au-SR-Au-SR)-. Also, the observed peak fragmentations in the MALDI spectrum (Figure 2, panel (IV)) provided more detail about possible structural composition. As shown in the panel (IV), some fragments can be recognized from the peak mass differences, and can be assigned as $Au(SC_4H_9)_2$ and 3×$AuSC_4$. The loss of a $Au(SC_4H_9)_2$ derivative is energetically favourable.[38] Both these mass features support the presence of the known staple motifs building up in the structural $Au_{23}(SC_4H_9)_{16}$ cluster compositions. All features are indicative of Au-SR staples in a core-shell system observed in the MS experiment.[47, 48] With these fragmentations taken into the consideration, the data suggests that the cluster structure likely includes staple motif structure similar to $Au_{25}(SR)_{18}$ and $Au_{38}(SR)_{24}$[22, 25, 49]. The Au_{25} and Au_{38} clusters includes Au_{13} and Au_{23} cores and their shell structures ($Au_{12}(SR)_{18}$ and $Au_{15}(SR)_{24}$) are composed of $Au(SR)_2$ and $Au_2(SR)_3$. Pei and Zeng have introduced a general structural formula for predicting the structural configuration in a cluster including: $[Au]_{a+a'}[Au(SR)_2]_b[Au_2(SR)_3]_c[Au_3(SR)_4]_d[Au_4(SR)_5]_e$ where a, a', b, c, d and e are integers that satisfy certain constraints.[50] Following the suggested structural formula and considering the mass evidence, there are two possible proposed structural formula for $Au_{23}(SC_4H_9)_{16}$: $[Au]_{14}[Au(SR)_2]_5[Au_2(SR)_3]_2$ and $[Au]_{13}[Au(SR)_2]_2[Au_2(SR)_3]_4$. Based on the theoretical studies, $[Au]_{13}[Au(SR)_2]_2[Au_2(SR)_3]_4$ with more symmetrical structure has lower energy and higher stability. Mass spectrometry along with DFT calculations provided evidence that the cluster with $[Au_{13}]$ core is more probable because of higher stability.[38]

The MS evidence suggests a possible core-shell structure for $Au_{23}(SC_4H_9)_{16}^-$, therefore a super-atom closed-shell

structure model can be tested.[51] In this model n* is representing the required number of electrons contributed in closed shell superatom of the metallic core: $n^*=N_A-M-z$. N_A is number of metal atoms, M is number of ligands and z is charge of the cluster. Considering Au_{23} decorated with $(SR)_{16}$ and including a negative charge, due to the presence of TOA, n* (shell-closing electronic count) can be calculated: n*=23-16+1=8e. This could be reasonable confirmation of the electronic stability of this cluster. The eight electron rule is in agreements with noble-gas super-atom logic, where Au-SR molecule-like cluster structure with closed electronic valence shell, following maximum occupancy in noble gas electronic configuration with 2, 8, 18, 34, 58 and 92 as magic values.[51] Recent density function theory (DFT) calculations based on the crystal structure of negatively charged Au_{23} protected with cyclohexane thiol, Jin and co-workers argued that although $Au_{23}(SR)_{16}^-$ follows the 8e rule, the origin of the HOMO orbitals are mainly constructed by atomic Au orbitals.[39]

^{1}HNMR study.

The two purified fractions were also studied with ^{1}HNMR spectroscopy using $CDCl_3$ as the solvent to assign possible interactions between the protecting ligands. Figure S2 shows the ^{1}HNMR spectra of the free ligand (a), tetra-*n*-octylammonium bromide (TOABr) (b), acetonitrile fraction (c) and dichloromethane fraction (d) in $CDCl_3$. The ^{1}HNMR spectra of the two fractions revealed similar patterns, which show a triplet due to TOA methyl groups at 0.9 ppm, high multiplicity in the range of 1.18-1.9 ppm and a triplet at 3.3 ppm for the α-methylenes in $-N^+-\mathbf{CH_2}-CH_2-$. By comparing the spectra (a), (b) and (c/d), it can be recognized that the protons in the range 1.18-1.9 ppm are due to the methyl protons of $(SC(CH_3)_3)$ and the methylene protons of TOA counter ion. Both spectra of the two fractions clearly show the presence of tetra-*n*-octylammonium (TOA^+) as the counter ion, consistent with the clusters being negatively charged.

The spectra of the both fractions show similar features, which is an indication of small clusters with molecule-like nanostructures.[52] Due to the presence of the TOA and its methylene protons peak overlaps with the ligands methyl groups further 1D-^{1}HNMR studies was difficult. Therefore, two dimensional double quantum filter cosy (2D-gDQCOSY) technique were employed for further NMR spectroscopic analyses . The obtained spectra showed there is the expected strong H-H correlation for TOA, while the methyl groups in the tert-butyl thiolate ligands do not have any apparent interaction on each other (see Figure S4).

Electrochemistry and photoluminescence of $Au_{23}(SC_4H_9)_{16}^-$.

The electrochemistry of the molecule-like gold clusters including $Au_{25}(SR)_{16}$, $Au_{38}(SR)_{24}$ and $Au_{144}(SR)_{60}$ have been the focus of many studies.[5, 53-57] Here, based on the novelty of the Au_{23} clusters, the electrochemistry of both fractions were also studied. The experiments have been conducted in Ar-saturated dichloromethane containing 1.0 mM of the $Au_{23}(SC_4H_9)_{16}^-$ cluster with 0.1 M $TBAPF_6$ as the supporting electrolyte. The open circuit potential of both clusters showed negative values (-190 and -170 mV), which is a further indication of presence of negative charge on the clusters as suggested by the ^{1}HNMR spectra.[58]

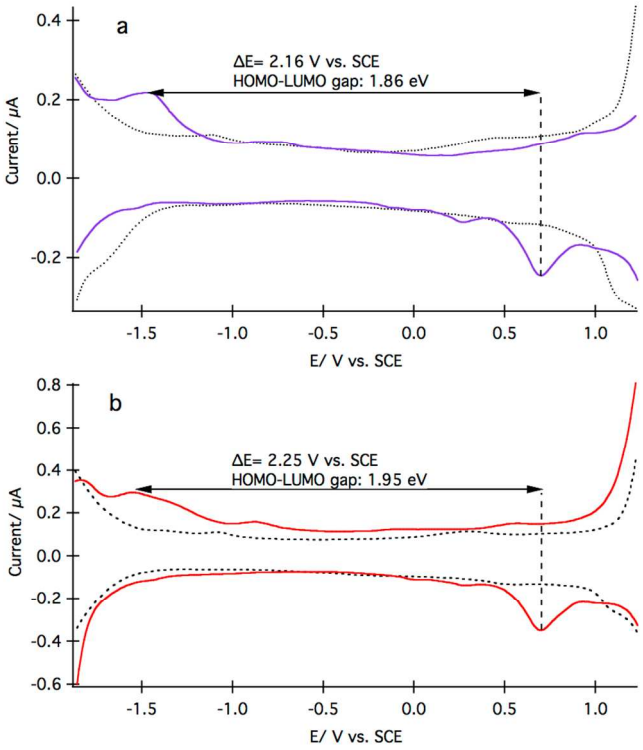

Figure 3. Differential pulse voltammograms (DPVs) of (a) acetonitrile and (b) dichloromethane fractions obtained in dichloromethane containing 0.1 M tetra-*n*-butylammonium hexaflourophosphate ($TBAPF_6$) as supporting electrolyte. Dashed lines show background DPVs in the absence of the clusters in the same solution. Scan rate: 50 mV/s, T=25°C.

Differential pulse voltammograms (DPVs) of both samples show two irreversible peaks at 0.74 and -1.58 V *vs*. SCE in the course of oxidative and reductive potential scans (Figure 3). The electrochemical HOMO-LUMO gap were calculated from the first oxidation and reduction potential differences. The HOMO-LUMO gap calculated after charge correction[54] *ca*. 1.86 and 1.95 eV for acetonitrile and dichloromethane fractions, which is close to the value estimated through the UV-Vis spectroscopy studies. Cyclic voltammetry (CV) of both cluster samples conducted in both the oxidation and reduction potential directions showed that the oxidation peak is well pronounced after reducing the clusters. (Figure 4 and Fig. S5).

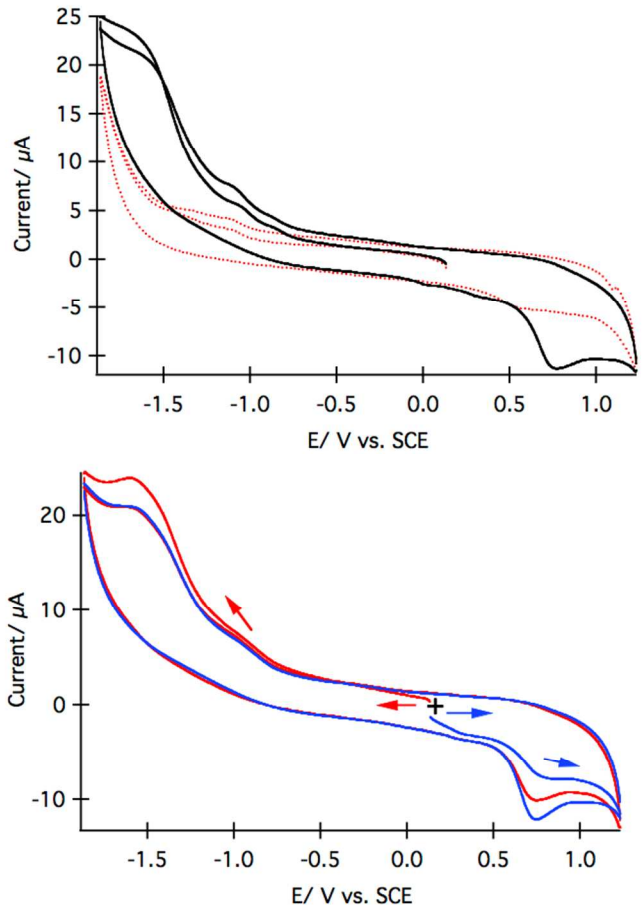

Figure 4 Cyclic voltammograms (CVs) of dichloromethane fraction obtained in dichloromethane containing 0.1 M tetra-*n*-butylammonium hexaflourophosphate ($TBAPF_6$) as supporting electrolyte. (Top) dotted lines show background CV in the absence of the clusters and solid line in the presence of cluster in the same solution. Bottom voltammograms show (the blue) scanning potential towards the positive and (the red) negative values. Scan rate: 100 mV/s, T=25°C.

This can be due to the capability of the electronic configuration to accept electron(s), which is favourable compare to removing electron(s). This observation was also tested using multi-cyclic potential scans (Fig. S7). It is worth nothing that the observed electrochemical behaviour of $Au_{23}(SC_4H_9)_{16}^-$ is differentiated from both $Au_{25}(SR)_{18}$ and $Au_{38}(SR)_{24}$ clusters, due to the fact that in both Au_{25} and Au_{38} clusters the HOMO orbitals have p-character properties, while DFT calculations on Au_{23}^- showed that for this cluster the HOMO orbitals are mostly constructed of the atomic orbitals of gold, although the Jin suggests that the HOMO is not a d-like orbital.[39] Similar quasi/irreversible electrochemical behaviour have been reported for $Au_{20}(SC_2H_4Ph)_{16}$ and $Au_{24}(SC_2H_4Ph)_{20}$ clusters, with generally a broad peak at ~ -1.0 V *vs.* Ag/AgCl.[59] One can conclude that the electronic (and even crystal) structure of Au_{20}, Au_{23} and Au_{24} are similar in terms of origin of the HOMO and LUMO orbitals locations and properties.

Further optical properties have been investigated using photoluminescence (PL) spectrometry. The PL spectra were obtained from the sample solutions in chloroform using a CCD camera (Andor technology) spectrograph instrument. The samples were excited at 532 nm using a laser source.

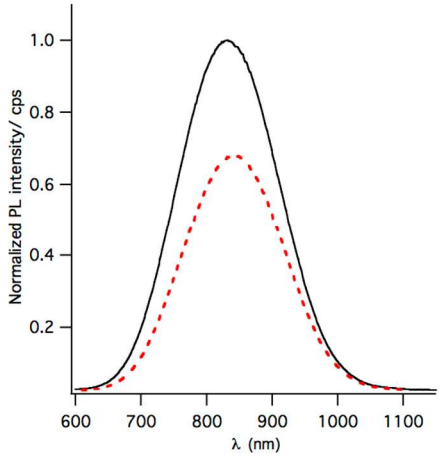

Figure 5. Photoluminescence of acetonitrile (solid line) and dichloromethane (dashed-line) fractions dissolved in $CHCl_3$ (C= 0.028 mM), excitation at 532 nm.

Figure 5 shows the PL spectra with peaks in the near-infrared (NIR) region at 830 and 838 nm for the acetonitrile and dichloromethane fractions at room temperature, respectively. The PL spectra were normalized to their absorption at 532 nm. The NIR emission is characteristic of small clusters [60] such as $Au_{25}(SR)_{18}$,[61] $Au_{38}(SR)_{24}$[62] and $Au_{144}(SR)_{60}$.[63] The emission wavelength supports the similarity of the excitation and emission processes of these systems with close HOMO-LUMO energy gaps. The PL intensity difference between these two fractions is likely related to the probability of the photoelectron excitation(s) through the HOMO-LUMO gaps. The acetonitrile fraction has a slightly smaller HOMO-LUMO gap, resulting in relatively higher PL intensity compared to the dichloromethane fraction.

Circular dichroism (CD) of both samples examined in chloroform, which showed no activity.

Powder X-ray diffraction.

Powder X-ray diffraction (PXRD) of the acetontrile fraction is shown in Figure 6. The inset of Figure 6 shows the peak at 39.8, fitted with one broad (Gussian) symmetric peak. The dichloromethane fraction PXRD was identical. The peak shape, position and peak width are characteristic of nano-crystalline structure of the sample.[64 65] The obtained XRD features are similar to the reported $Au_{20}(SR)_{16}$ $Au_{24}(SR)_{20}$[21] and $Au_{30}(SR)_{18}$[27].

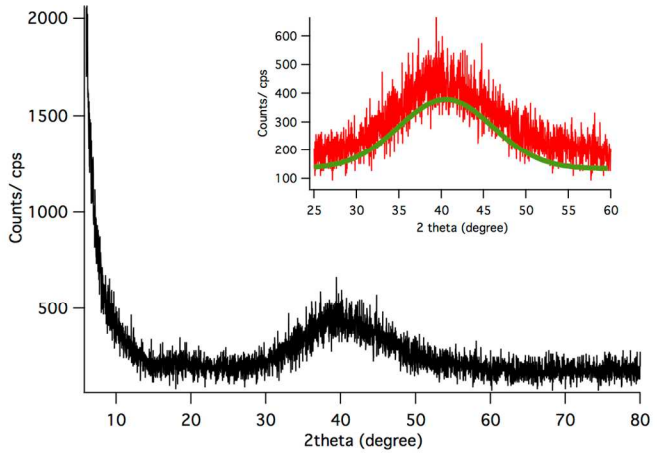

Figure 6. Powder X-ray diffraction (PXRD) spectrum of the acetonitrile fraction of the $Au_{23}(SC_4H_9)_{16}$.TOA. The inset shows the fitted main peak.

CONCLUSIONS

New mono-dispersed negatively charged $Au_{23}(HSC(CH_3)_3)_{16}$ clusters are prepared in a one phase/ one pot synthesis. Two clusters were isolated in two fractions with one exhibiting a different solubility in acetonitrile and dichloromethane. Both fractions are soluble in dichloromethane, chloroform, THF, acetone and toluene. ESI and MALDI mass spectrometry techniques verified the structural formula as $Au_{23}(SC(CH_3)_3)_{16}$, with $Au(SR)_2$ and $Au_2(SR)_3$ stable motifs. The optical and electrochemical HOMO-LUMO gap showed a good agreement, with *ca*. 1.86 and 1.95 eV for the acetonitrile and dichloromethane fractions, respectively. ^{1}HNMR spectrometry verifies that tetra-*n*-octylammonium ion (TOA^+) is present in the final clusters as a counter ion, and thus the clusters are negatively charged. Photoluminescence measurements in chloroform show a peak at 830 and 838 nm, for acetonitrile and dichloromethane fractions, respectively. The PL intensity difference between the two fractions is related to the HOMO-LUMO energy gaps. Due to the similarities of all the characterisation data, with only subtle differences, the two fractions likely only differ either in the relative orientation (bonding) of the protecting ligands around the gold core or some other structural distortion. Continued studies like this using bulky ligands such as $HSC(CH_3)_3$ are providing additional insight into the effect of ligand on the structure and inherent properties of small Au clusters.

Acknowledgements

NSERC and the Department of Chemistry for financial support. Mr. D. Hairsine and Dr. Mathew Willans for their technical assistance for MS and NMR spectroscopic experiments. G. Yao and V. Dehnavi for assistance with the XRD experiments.

Notes and references

1 Y. Zhu, H. Qian and R. Jin, *J. Mater. Chem.*, 2011, **21**, 6793-6799.
2 A. Kubacka, M. Fernandez-Garcia and G. Colon, *Chem. Rev.*, 2011, **112**, 1555-1614.
3 G. V. Hartland, *Chem. Rev.*, 2011, **111**, 3858-3887.
4 L. H. Reddy, J. L. Arias, J. Nicolas and P. Couvreur, *Chem. Rev.*, 2012, **112**, 5818-5878.
5 K. N. Swanick, M. Hesari, M. S. Workentin and Z. Ding, *J. Am. Chem. Soc.*, 2012, **134**, 15205-15208.
6 K. Saha, S. S. Agasti, C. Kim, X. Li and V. M. Rotello, *Chem. Rev.*, 2012, **112**, 2739-2779.
7 M.-C. Daniel and D. Astruc, *Chem. Rev.*, 2003, **104**, 293-346.
8 R. W. Murray, *Chem. Rev.*, 2008, **108**, 2688-2720.
9 A. S. Thakor, J. Jokerst, C. Zavaleta, T. F. Massoud and S. S. Gambhir, *Nano Lett.*, 2011, **11**, 4029-4036.
10 M. J. Hostetler, J. E. Wingate, C.-J. Zhong, J. E. Harris, R. W. Vachet, M. R. Clark, J. D. Londono, S. J. Green, J. J. Stokes, G. D. Wignall, G. L. Glish, M. D. Porter, N. D. Evans and R. W. Murray, *Langmuir*, 1998, **14**, 17-30.
11 C. Liu, G. Li, G. Pang and R. Jin, *RSC Advances*, 2013, **3**, 9778-9784.
12 R. Jin, *Nanoscale*, 2010, **2**, 343-362.
13 T. G. Schaaff, G. Knight, M. N. Shafigullin, R. F. Borkman and R. L. Whetten, *J. Phys. Chem. B*, 1998, **102**, 10643-10646.
14 X.-K. Wan, Z.-W. Lin and Q.-M. Wang, *J. Am. Chem. Soc.*, 2012, **134**, 14750-14752.
15 S. Kumar and R. Jin, *Nanoscale*, 2012, **4**, 4222-4227.
16 A. H. Holm, M. Ceccato, R. L. Donkers, L. Fabris, G. Pace and F. Maran, *Langmuir*, 2006, **22**, 10584-10589.
17 Y. Negishi, U. Kamimura, M. Ide and M. Hirayama, *Nanoscale*, 2012, **4**, 4263-4268.
18 M. Brust, M. Walker, D. Bethell, D. J. Schiffrin and R. Whyman, *Chem. Commun.*, 1994, 801-802.
19 Z. Wu, J. Suhan and R. Jin, *J. Mater. Chem.*, 2009, **19**, 622-626.
20 M. Zhu, H. Qian and R. Jin, *J. Am. Chem. Soc.*, 2009, **131**, 7220-7221.
21 M. Zhu, H. Qian and R. Jin, *J. Phys. Chem. Lett.*, 2010, **1**, 1003-1007.
22 M. Zhu, C. M. Aikens, F. J. Hollander, G. C. Schatz and R. Jin, *J. Am. Chem. Soc.*, 2008, **130**, 5883-5885.
23 C. Zeng, T. Li, A. Das, N. L. Rosi and R. Jin, *J. Am. Chem. Soc.*, 2013, **135**, 10011-10013.
24 C. Zeng, H. Qian, T. Li, G. Li, N. L. Rosi, B. Yoon, R. N. Barnett, R. L. Whetten, U. Landman and R. Jin, *Angew. Chem. Inter. Ed.*, 2012, **51**, 13114-13118.
25 H. Qian, W. T. Eckenhoff, Y. Zhu, T. Pintauer and R. Jin, *J. Am. Chem. Soc.*, 2010, **132**, 8280-8281.
26 P. D. Jadzinsky, G. Calero, C. J. Ackerson, D. A. Bushnell and R. D. Kornberg, *Science*, 2007, **318**, 430-433.
27 D. Crasto and A. Dass, *J. Phys. Chem. C*, 2013, **117**, 22094-22097.
28 R. C. Price and R. L. Whetten, *J. Am. Chem. Soc.*, 2005, **127**, 13750-13751.
29 J.-i. Nishigaki, R. Tsunoyama, H. Tsunoyama, N. Ichikuni, S. Yamazoe, Y. Negishi, M. Ito, T. Matsuo, K. Tamao and T. Tsukuda, *J. Am. Chem. Soc.*, 2012, **134**, 14295-14297.
30 P. R. Nimmala and A. Dass, *J. Am. Chem. Soc.*, 2011, **133**, 9175-9177.
31 P. J. Krommenhoek, J. Wang, N. Hentz, A. C. Johnston-Peck, K. A. Kozek, G. Kalyuzhny and J. B. Tracy, *ACS Nano*, 2012.
32 S. Chen and R. W. Murray, *Langmuir*, 1998, **15**, 682-689.

33 J.-i. Nishigaki, S. Yamazoe, S. Kohara, A. Fujiwara, W. Kurashige, Y. Negishi and T. Tsukuda, *Chem. Commun.*, 2014, **50**, 839-841.
34 H. Yao, K. Miki, N. Nishida, A. Sasaki and K. Kimura, *J. Am. Chem. Soc.*, 2005, **127**, 15536-15543.
35 C. M. Aikens, *J. Phys. Chem. A*, 2009, **113**, 10811-10817.
36 E. B. Guidez, V. P. Makinen, H. J. Hakkinen and C. M. Aikens, *J. Phys. Chem. C*, 2012, **116**, 20617-20624.
37 G.-T. Bae and C. M. Aikens, *J. Phys. Chem. A*, 2013, **117**, 10438-10446.
38 O. Lopez-Acevedoa and H. Hakkinen, *Eur. Phys. J. D*, 2011, **63**, 311-314.
39 A. Das, T. Li, K. Nobusada, C. Zeng, N. L. Rosi and R. Jin, *J. Am. Chem. Soc.*, 2013, **135**, 18264-18267.
40 S. Sahami and M. J. Weaver, *J. Electroanal. Chem. and Interfac. Electrochem.*, 1981, **122**, 155-170.
41 N. K. Chaki, Y. Negishi, H. Tsunoyama, Y. Shichibu and T. Tsukuda, *J. Am. Chem. Soc.*, 2008, **130**, 8608-8610.
42 L. A. Angel, L. T. Majors, A. C. Dharmaratne and A. Dass, *ACS Nano*, 2010, **4**, 4691-4700.
43 C. A. Fields-Zinna, M. C. Crowe, A. Dass, J. E. F. Weaver and R. W. Murray, *Langmuir*, 2009, **25**, 7704-7710.
44 J. B. Tracy, M. C. Crowe, J. F. Parker, O. Hampe, C. A. Fields-Zinna, A. Dass and R. W. Murray, *J. Am. Chem. Soc.*, 2007, **129**, 16209-16215.
45 A. Dass, P. R. Nimmala, V. R. Jupally and N. Kothalawala, *Nanoscale*, 2013, **5**, 12082-12085.
46 A. Dass, K. Holt, J. F. Parker, S. W. Feldberg and R. W. Murray, *J. Phys. Chem. C*, 2008, **112**, 20276-20283.
47 A. Dass, G. R. Dubay, C. A. Fields-Zinna and R. W. Murray, *Anal. Chem.*, 2008, **80**, 6845-6849.
48 S. M. Reilly, T. Krick and A. Dass, *J. Phys. Chem. C*, 2009, **114**, 741-745.
49 M. W. Heaven, A. Dass, P. S. White, K. M. Holt and R. W. Murray, *J. Am. Chem. Soc.*, 2008, **130**, 3754-3755.
50 Y. Pei and X. C. Zeng, *Nanoscale*, 2012, **5**, 4054-4072.
51 M. Walter, J. Akola, O. Lopez-Acevedo, P. D. Jadzinsky, G. Calero, C. J. Ackerson, R. L. Whetten, H. Gronbeck and H. Hakkinen, *Proceed. Nat. Acad. of Sci.*, 2008, **105**, 9157-9162.
52 K. Salorinne, T. Lahtinen, J. Koivisto, E. Kalenius, M. Nissinen, M. J. Pettersson and H. J. Hakkinen, *Anal. Chem.*, 2013, **85**, 3489-3492.
53 S. Antonello, M. Hesari, F. Polo and F. Maran, *Nanoscale*, 2012, **4**, 5333-5342.
54 D. Lee, R. L. Donkers, G. Wang, A. S. Harper and R. W. Murray, *J. Am. Chem. Soc.*, 2004, **126**, 6193-6199.
55 S. Antonello, A. H. Holm, E. Instuli and F. Maran, *J. Am. Chem. Soc.*, 2007, **129**, 9836-9837.
56 O. Toikkanen, V. Ruiz, G. Ronnholm, N. Kalkkinen, P. Liljeroth and B. M. Quinn, *J. Am. Chem. Soc.*, 2008, **130**, 11049-11055.
57 B. M. Quinn, P. Liljeroth, V. Ruiz, T. Laaksonen and K. s. Kontturi, *J. Am. Chem. Soc.*, 2003, **125**, 6644-6645.
58 Y. Song, A. S. Harper and R. W. Murray, *Langmuir*, 2005, **21**, 5492-5500.
59 X. Zhu, S. Jin, S. Wang, X. Meng, C. Zhu, M. Zhu and R. Jin, *Chem. – An Asian J.*, 2013, **8**, 2739-2745.
60 G. Wang, T. Huang, R. W. Murray, L. Menard and R. G. Nuzzo, *J. Am. Chem. Soc.*, 2004, **127**, 812-813.
61 Z. Wu and R. Jin, *Nano Lett.*, 2010, **10**, 2568-2573.
62 J. T. v. Wijngaarden, O. Toikkanen, P. Liljeroth, B. M. Quinn and A. Meijerink, *J. Phys. Chem. C*, 2010, **114**, 16025-16028.
63 T. P. Bigioni, R. L. Whetten and Ö. Dag, *J. Phys. Chem. B*, 2000, **104**, 6983-6986.
64 C. L. Cleveland, U. Landman, M. N. Shafigullin, P. W. Stephens and R. L. Whetten, *Zeitschrift für Physik D Atoms, Molecules and Clusters*, 1997, **40**, 503-508.
65 R. C. Price, *Nanocrystalline Gold Arylthiolate Molecules, Ph.D. Dissertation, Georgia Institute of Technology*, 2006.

Department of Chemistry, The University of Western Ontario, London, N6A 5B7, CANADA
Address correspondence to: mworkent@uwo.ca.

† Electronic Supplementary Information (ESI) available: Expanded ESI mass spectrum, Expanded 1D-^{1}HNMR, 2D-gDOCOSY NMR of dichloromethane fraction, Cyclic voltammograms of acetonitrile dichloromethane fraction. Multicyclic voltammograms of dichloromethane fraction. See DOI: 10.1039/b000000x/

Table of Contents:

$Au_{23}(SC(CH_3)_3)_{16}^-$.$TOA^+$ clusters decorated with *t*-butyl thiolate lignads have been prepared using one-pot/one-step reaction protocol. The resulting clusters were differentiated only by their differing solubility in acetonitrile..

Journal Name

RSCPublishing

ARTICLE